Environmental Science & Technology

Article

pubs.acs.org/est

Photocatalytic Degradation Efficiency and Mechanism of Microcystin-RR by Mesoporous Bi_2WO_6 under Near Ultraviolet Light

Peng Chen, Lingyan Zhu,* Shuhong Fang, Chunying Wang, and Guoqiang Shan

College of Environmental Science and Engineering, Key Laboratory of Pollution Processes and Environmental Criteria, Ministry of Education, Tianjin Key Laboratory of Environmental Remediation and Pollution Control, Nankai University, Tianjin 300071, People's Republic of China

Supporting Information

ABSTRACT: Microcystin-RR (MC-RR) is one of the most common cyanotoxin microcystins in fresh water and is of great concern due to its potential hepatotoxicity. In the present study, Bi_2WO_6 was synthesized with a hydrothermal method by varying the pH of the reaction solution in the range of 1−11. The surface area of the catalysts decreased, but the crystallinity and crystal size increased with the pH. The adsorption and degradation capacities of the catalysts decreased with increasing the preparation solution pH. The Bi_2WO_6 prepared at pH 1 (Bi_2WO_6-pH1) displayed the highest adsorption and degradation capacity to MC-RR even though it consisted of randomly aggregated particles. Nearly 100% of MC-RR at 10 mg L^{-1} was removed after 30 min of irradiation of near-ultraviolet light (300−400 nm) in a solution with Bi_2WO_6 concentration of 0.2 g L^{-1}. The photodegradation efficiency of Bi_2WO_6-pH1 was greater in acid medium than in basic solutions. Several intermediate products were observed and identified by liquid chromatography/mass spectrometry/mass spectrometry, and a unique photodegradation pathway was proposed. It was assumed that a photo-Kolbe process happened at the site carboxyl acid group of the D-Glu residue by the photogenerated holes, producing a hydroperoxyl product at m/z 513.8. This intermediate could be further decomposed to an alcohol product at m/z 505.8 and a ketone product at m/z 504.8. The aromatic ring and diene bond of the Adda chain could also be attacked by the holes and form phenol and diol products.

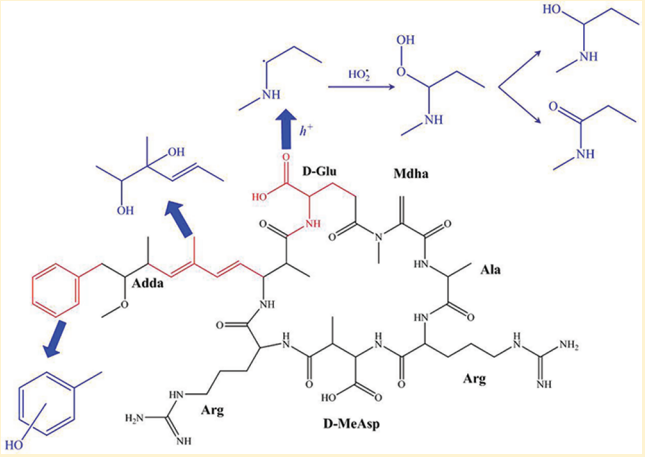

INTRODUCTION

The occurrence of blue algae blooms increases with the water eutrophication in lakes, producing a series of cyanotoxins, such as microcystins (MCs) and nodularins. MCs are mainly produced by the strains *Microcystis sp.*, *Anabaena sp.*, *Planktothrix sp.*, *Nostoc sp.*, and so forth[1] and may cause adverse effects to bioorganisms and humans by inhibiting protein phosphatases.[2−4] More than 90 kinds of MCs have been identified up to now,[5] and they possess the same generic cyclic heptapeptides structure (See Figure S1 in the Supporting Information) with two of the seven amino acids being variable (position X and Z). Among the various MCs, microcystin-RR (MC-RR) is the most common one with two arginine residues (Arg) at position X and Z and is predominant in many lakes in China, such as Taihu Lake and Chaohu Lake.[6] The presence of MC-RR in water, especially in drinking water, is of great concern, since chronic exposure may cause tumor promotion.[7,8]

MCs are very stable in the environment because of their cyclic structure.[9] They can be decomposed slowly by acids, alkalines, heating, or biological methods.[10] It was reported that MCs could be destroyed by advanced oxidation technologies (AOT) such as UV radiation,[11] TiO_2 photocatalysis,[12−15] Fenton oxidation,[16] and ultrasonic irradiation.[17] Most of the studies are on microcystin-LR (MC-LR),[18−20] and a few have been conducted to MC-RR. Usually, the main reaction sites of MCs are the aromatic ring, diene bond, methoxy group of the Adda chain, the double bond of Mdha residue, and the free carboxyl acid via hydroxyl radical (•OH) and sulfate radical attack.[14,21−23] Since MC-LR and MC-RR have two different amino acids, the degradation process and pathway may be quite different. Lawton et al. compared the degradation of four kinds of MCs using TiO_2 photocatalyst and found that MC-RR was the most difficult to be destroyed.[15]

Bismuth tungstate (Bi_2WO_6) is a new kind of photocatalyst and displays great photocatalytic capacity under simulated solar light and visible light.[24,25] It was reported in previous studies that Bi_2WO_6 cannot generate •OH, which is reported to be the

Received: October 13, 2011
Revised: January 8, 2012
Accepted: January 17, 2012
Published: January 17, 2012

main active species for oxidative degradation when TiO_2 and other catalysts are utilized.[26,27] The main active species were reported to be photogenerated holes (h^+), conduction band electrons (e_{CB}^-) and superoxide radical ($O_2\bullet^-$) in the reaction system with Bi_2WO_6.[24,26,28] Bi_2WO_6 could be synthesized using the hydrothermal method, and its properties are highly dependent on pH of the hydrothermal solution. For example, Wang et al.[24] reported that Bi_2WO_6 prepared at pH 11 displayed the highest crytallinity and photodegradation efficiency to Bisphenol A (BPA) under simulated solar light while Amano et al.[28] discovered that Bi_2WO_6 prepared at acid condition was better than alkaline condition when it was used to degrade acetic acid.

The purpose of this study was to investigate the photocatalytic degradation of MC-RR using Bi_2WO_6 as catalyst, which was prepared using the hydrothermal method with pH varying in the range 1−11. The synthesized catalysts were characterized comprehensively and were tested for the capacity to degrade MC-RR under near-ultraviolet light irradiation. Liquid chromatography/mass spectrometry/mass spectrometry (LC/MS/MS) was used to identify the structure of the intermediates produced during the process of photodegradation. The degradation pathway was discussed based on the information of the produced intermediates.

EXPERIMENTAL SECTION

Materials and Reagents. MC-RR standard was purchased from Express Technology Co., Ltd., China. $Bi(NO_3)_3{\cdot}5H_2O$, $Na_2WO_4{\cdot}2H_2O$, NaOH, and HNO_3 (analytical grade) were purchased from Chemical Technology Co., Ltd., Tianjin, China. TiO_2 particles (P25, Degussa) were purchased from Degussa Corporation, Germany. Methanol used for the mobile phase of high performance liquid chromatography (HPLC) analysis was purchased from Concord Technology Co., Ltd., Tianjin, China. Acetonitrile (HPLC grade) and formic acid used for liquid chromatography coupled with mass spectrometer (LC-MS) analysis were purchased from Dikma Technology Inc., USA.

Preparation and Characterization of Photocatalyst Bi_2WO_6. Bi_2WO_6 was prepared using the hydrothermal method described by Wang et al.[24] Briefly, 20 mL of sodium tungstate solution at 0.05 mol L^{-1} was added into 20 mL of bismuth nitrate solution at 0.10 mol L^{-1}. The pH of the solution was adjusted with 1 M NaOH solution to 1.0, 5.0, 7.0, and 11.0. The suspension was transferred to a 50 mL Teflon-lined autoclave and then heated to 140 °C for 20 h in an oven. The precipitates were collected by centrifugation, washed with water and ethanol, and dried at 120 °C for 4 h.

Crystallographic information of the products was obtained by X-ray diffraction (XRD, Rigaku D/MAX-RB, Cu Kα radiation, Japan). Morphology of the photocatalyst was examined by a 1530VP scanning electron microscope (SEM). Brunauer−Emmett−Teller (BET) surface area and pore size measurements were performed on an autosorb-1-MP 1530VP automatic surface area and pore size analyzer. The pH of the point of zero charge (pH_{PZC}) of Bi_2WO_6 was determined by the pH drift method.[29]

Photocatalytic Reaction. The photocatalytic experiments were performed in a photochemical reactor (XPA-7, Xujiang, Nanjing, China). Five mL of 10 mg L^{-1} MC-RR solution was added into a 20 mL quartz glass vial, in which Bi_2WO_6 was added with a loading amount at 0.2 g L^{-1}. For comparison, the same amount of TiO_2 was also used to degrade MC-RR. The mixture was magnetically stirred in the dark for 30 min to ensure adsorption−desorption equilibrium of MC-RR on the catalysts (a preliminary experiment indicated that 30 min was enough for the adsorption equilibrium). Then, the mercury lamp was turned on to initiate the photodegradation under near-ultraviolet light (300−400 nm, 100 W low pressure mercury lamp with 365 nm light filter). The lamp was warmed up for 10 min to ensure constant illumination intensity. Approximate 0.5 mL of the reaction solution was withdrawn from the reactor and centrifuged under 10 000 rpm before MC-RR analysis. At the end of reaction, the residual catalysts were extracted using 0.5 mL of 0.01 mol L^{-1} NaOH for three times to determine the amount of MC-RR adsorbed on the solids.

Analysis of MC-RR and Intermediates. MC-RR in the reaction solution was measured by HPLC (Agilent 1260) with the UV detector at 238 nm wavelength. The analytical conditions were as follows: column was 150 mm × 4.6 mm I.D. (Waters XTerra C18 column); the mobile phase was 55:45 (v/v) methanol and 0.1% trifluoroacetic acid aqueous solution; flow rate was set as 0.6 mL min^{-1}; oven temperature was set at 40 °C. The reaction intermediates were monitored and identified by LC-MS system (Agilent 1200 with 6310 ion trap mass spectrometer) with full scan from m/z 100 to 1200 in positive electrospray ionization (ESI) mode. The analytical column used was 150 mm × 2.1 mm I.D. (Waters XTerra C18 column) with a gradient elution of 0.05% formic acid aqueous solution (A) and 0.05% formic acid acetonitrile solution (B) at a flow rate of 0.25 mL min^{-1} with column temperature of 40 °C. Gradient elution was programmed as 20% B for 9 min, then from 20% B to 38% B in 3 min, holding for 7 min, finally to 20% B in 1 min, holding for 5 min. The LC/MS parameters were set as follows: capillary voltage, 3000 V; capillary exit voltage, 143.5 V; nebulizer, 25.0 psi; flow of dry gas, 8.0 L min^{-1}; dry temperature, 350 °C. LC/MS/MS was used to identify the structure of the stable intermediate products during the reaction.

RESULTS AND DISCUSSION

Bi_2WO_6 Characterization. Figure 1(a) shows the XRD patterns of Bi_2WO_6 prepared at different hydrothermal pHs. The diffraction peaks of the products are consistent with those of russellite Bi_2WO_6 [JCPDS No. 39-0256]. This agrees with the result reported by Wang et al.[24] The crystallite size was calculated by the Debye−Scherrer equation, and the results are listed in Table 1. It is in the ranges 8.8−14.4, 9.6−15.2, 10.6−14.6, and 15.4−18.2 nm for the products prepared at pH 1, 5, 7, and 11, respectively. The crystallite size increases with increasing pH of the hydrothermal reaction solution. As reported by Wang et al.,[24] the morphology of Bi_2WO_6 is highly dependent on the pH of the reaction solution. As shown in Figure S2 of the Supporting Information, Bi_2WO_6 prepared at pH 1 (Bi_2WO_6−pH 1) mainly consists of a mixture of small spherical and randomly aggregated particles. At pH 5, the particles become bigger and sheet-shaped aggregates appear; at pH 7, large particles as hierarchical assemblies of multilayered flakes are observed; while at pH 11, it is mainly in large sheet-shaped morphology with multilayered flakes. Figure 1(b) shows the diffuse reflectance UV−vis spectra of Bi_2WO_6 prepared at different pHs. The light absorption edge of the prepared catalysts is between 420 and 450 nm, suggesting their potential photocatalytic activity under visible light. Bi_2WO_6−pH 1 displays the strongest light absorbance. As shown in Table 1, the S_{BET} decreases gradually from 48.8 to 42.4, 34.8, and 16.8 m^2 g^{-1} as the pH increases from 1 to 11. The pore size of Bi_2WO_6−pH 1 is in the mesoporous range 2−30 nm. The pH_{PZC} of Bi_2WO_6 increases from 4.1 to 8.6 as the pH increases from 1 to 11.

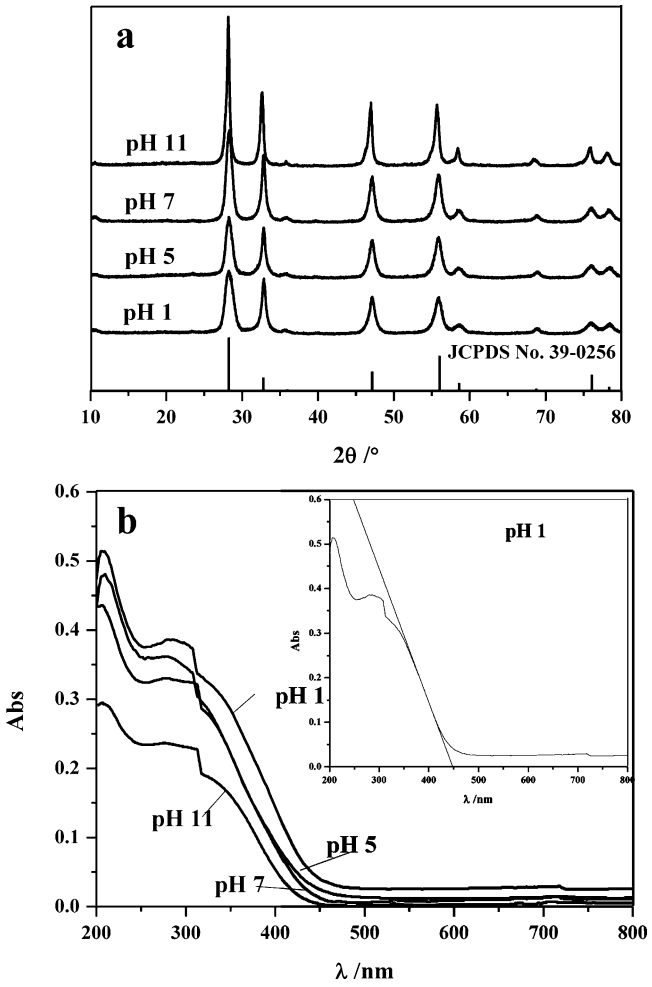

Figure 1. (a) XRD patterns of Bi_2WO_6 prepared at different hydrothermal pHs. (b) Diffuse reflectance UV–vis spectra of Bi_2WO_6 prepared at different hydrothermal pHs.

Table 1. Characteristics of Bi_2WO_6 Prepared at Different Hydrothermal pHs

prepared pH	pH 1	pH 5	pH 7	pH 11
crystallite size/nm	8.8–14.4	9.6–15.2	10.6–14.6	15.4–18.2
S_{BET} /m^2 g^{-1}	48.8	42.4	34.8	16.8
pH_{PZC}	4.1	4.6	5.3	8.6
E_g /eV	2.76	2.85	2.88	2.95
absorption edge/nm	450	435	430	420

Photodegradation of MC-RR by Bi_2WO_6 Prepared at Different pHs. Before irradiation, MC-RR was allowed to adsorb on the catalysts in the dark for 30 min, and the sorption kinetics are shown in Figure 2(a). The adsorption is very quick, and equilibrium is reached in 5 min. The adsorption capacity of Bi_2WO_6 prepared at specific hydrothermal conditions decreases as hydrothermal solution pH increases. About 25–30% MC-RR could be adsorbed by Bi_2WO_6–pH 1 while only about 8% is adsorbed by that prepared at pH 11. This is consistent with the order of their S_{BET} values. Bi_2WO_6–pH 1 has much larger surface area than those prepared at higher pH, providing more adsorption sites for MC-RR.

It was reported that UV light irradiation at 254 nm could cause isomerization of the diene bonds in MC-RR.[14] To avoid its isomerization, a 365 nm light filter was applied to ensure the

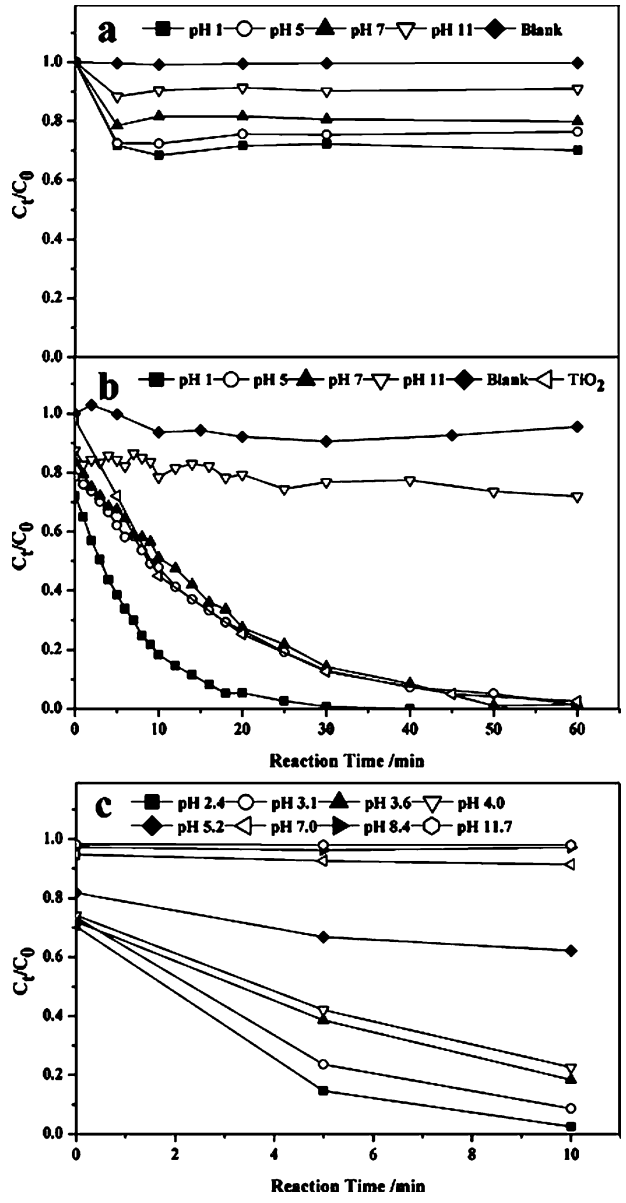

Figure 2. (a) Adsorption of MC-RR on Bi_2WO_6 prepared at different hydrothermal pHs. (b) Degradation kinetics of MC-RR by Bi_2WO_6 prepared at different hydrothermal pHs and P25 TiO_2 under near-ultraviolet light irradiation. (c) Effect of solution pH on the photodegradation of MC-RR by Bi_2WO_6–pH1. The amount of Bi_2WO_6 was set as 0.2 g L^{-1}, and the concentration of MC-RR was set as 10 mg L^{-1}.

irradiation light is in the range 300–400 nm. Figure 2(b) illustrates the degradation of MC-RR under near-ultraviolet irradiation by Bi_2WO_6 prepared at different pHs. Almost no MC-RR is decomposed in the control experiment without any catalyst. Bi_2WO_6–pH 1 displays much higher degradation efficiency to MC-RR than those prepared at higher pH and P25 TiO_2. MC-RR is almost completely removed in 30 min by Bi_2WO_6–pH 1. At the end of reaction, the amount of MC-RR adsorbed on the catalysts was determined. No MC-RR was detected in the Bi_2WO_6–pH 1 solids after irradiation for 30 min, suggesting that all adsorbed MC-RR was photocatalytically degraded. All the reactions follow pseudofirst order kinetics, and the kinetic rate constant (k) was calculated. The k decreases from 0.1333 min^{-1} for Bi_2WO_6–pH 1 to 0.0567 and 0.0533 min^{-1} for

dx.doi.org/10.1021/es2036338 | Environ. Sci. Technol. 2012, 46, 2345–2351

Bi_2WO_6 prepared at pHs 5 and 7, respectively. Almost no MC-RR was degraded by Bi_2WO_6 prepared at pH 11 in 30 min. As a comparison, the degradation of MC-RR by P25 TiO_2 was also investigated. As shown in Figure 2(b), the adsorption of MC-RR on P25 is negligible, agreeing with the results reported by Lawton et al.[15] The degradation rate constant k by P25 TiO_2 is 0.0698 min^{-1}, much lower than Bi_2WO_6–pH 1. The result is different from what is reported by Wang et al.,[24] who found that the photodegradation efficiency increased as the pH of the hydrothermal reaction solution increased from 4 to 11 and the catalyst prepared at pH 11 displayed the highest degradation efficiency to BPA (bisphenol A). Surface area and crystallinity are the most important factors to influence the photocatalytic activity.[24,30] A large surface area favors the sorption of substrates to the catalyst and leads to faster reaction. Many studies confirmed that adsorption of contaminants on photocatalysts is an important factor for effective photodecomposition.[31,32] The highest adsorption capacity of Bi_2WO_6–pH1 to MC-RR could result in its best photodegradation efficiency. However, due to the electrostatic repulsion force between BPA molecules and Bi_2WO_6 surface, the adsorption of BPA on Bi_2WO_6 was very weak, and there was no significant difference in adsorption capacity between the catalysts prepared at different pHs. Crystallinity became the dominant factor to affect the degradation efficiency of BPA. Amano et al.[28] also reported that the photocatalytic activity of Bi_2WO_6 increased with the surface area but was not dependent on the crystallinity. They also discovered Bi_2WO_6 prepared at acid condition was more effective than alkaline condition for the photocatalytic degradation of acetic acid. Herein, Bi_2WO_6–pH 1 was selected as the optimum catalyst and was used in the following experiments.

Effect of Initial pH of MC-RR Solution. The initial pH of the MC-RR solution could affect the degradation strongly, as shown in Figure 2(c). As the initial pH of the solution increases from 2.4 to 11.7, the degradation efficiency decreases significantly. The concentration of hydrogen ion (H^+) or hydroxide ion (OH^-) in aqueous solution may affect the deprotonation of both MC-RR and the catalysts, which in turn would affect the adsorption capacity and catalytic activity of the photocatalysts. Lawton et al. reported that hydrophobicity was the most important factor controlling the sorption of MC on the surface of TiO_2.[15] MC-RR shows very weak hydrophobicity as compared to MC-LR, due to its two polar Arg residues. The hydrophobic property of the Adda group in MC-RR helps its sorption on the surface of Bi_2WO_6. Due to the strong polarity, steric hindrance resulting from the long chain structure, and the electrostatic repulsion force of the two Arg groups, the Arg–MeAsp–Arg side tends to stay away while the Adda–Glu–Mdha side tends to approach the surface of Bi_2WO_6. The pKa of the free carboxyl group at the D-Glu side is 2.10.[15] In the studied pH range (2.4–11.7), the carboxyl group is fully deprotonated and negatively charged. The pH_{PZC} of Bi_2WO_6–pH 1 is 4.1. When the pH is lower than 4.1, the surface of Bi_2WO_6 is positively charged while it is negatively charged when above pH 4.1. Therefore, there is strong electrostatic attraction force between the negatively charged Glu–Mdha side of MC-RR and the positively charged Bi_2WO_6 surface when the pH is 2.4–4.0. Meanwhile, hydrogen bonds could be formed between them at low pH.[33] As a result, Bi_2WO_6 displays strong adsorption capacity to MC-RR at acidic conditions, leading to higher degradation efficiency, as shown in Figure 2(c). As the pH increases above 4.0, the surface of Bi_2WO_6 gradually becomes negatively charged. The electronic attraction becomes weak, and electronic repulsion predominates at basic conditions. As a result, the sorption of MC-RR on Bi_2WO_6 is impeded. The adsorption of MC-RR on Bi_2WO_6 at pH 7–11.7 is very weak, resulting in very low photodegradation efficiency. The results also suggest that photodegradation of MC-RR on Bi_2WO_6 is taking place on or very near the surface. It was reported that direct hole oxidation was the main reaction species for photodegradation when Bi_2WO_6 was used as a photocatalyst.[34] Since the holes are produced on the surface of Bi_2WO_6 and cannot spread into the solution, better adsorption would enhance the photodegradation by Bi_2WO_6.

Photodegradation Mechanism of MC-RR by Bi_2WO_6. No intermediate was detected by LC/MS/MS during the adsorption–desorption process. However, a number of intermediates were detected after irradiation for 2 min. Table S1 of the Supporting Information lists the retention times and molecular weights of the intermediates detected by LC/MS and their peak areas at different reaction times, while Figure 3 illustrates the time evolution of the main intermediates (m/z 439.8, 504.8, 505.8, 513.8, 527.8, 536.8) in the reaction solution. The structures of the main intermediates were identified by LC/MS/MS.

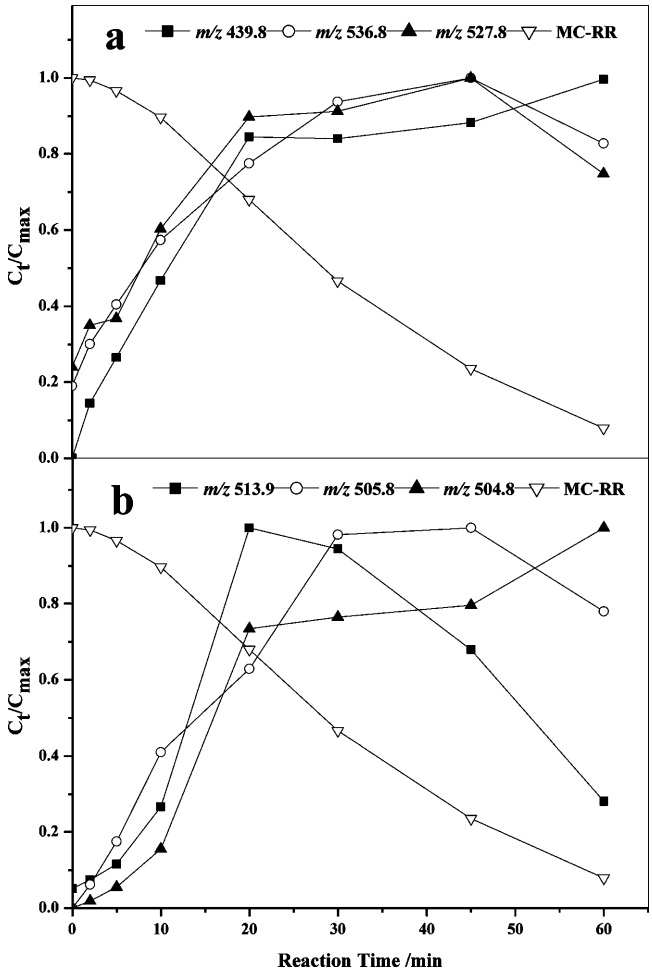

Figure 3. Time evolution of the major intermediates during the photodegradation. C_t is the concentration of one intermediate at reaction time t (min), and C_{max} is the maximum concentration of this intermediate. The amount of Bi_2WO_6 was set as 0.1 g L^{-1}; the concentration of MC-RR was set as 20 mg L^{-1}.

dx.doi.org/10.1021/es2036338 | Environ. Sci. Technol. 2012, 46, 2345–2351

The intermediate at m/z 513.8 was indentified to be a hydroperoxide product of MC-RR (The detailed information about its identification is shown in the Supporting Information, Figures S3−S6), m/z 505.8 to be an alcohol product (Supporting Information, Figures S7 and S8), and m/z 504.8 to be a ketone product (Supporting Information, Figures S9 and S10) based on the information generated by LC/MS/MS. The intermediates at m/z 513.8 (isomer A), 505.8, and 504.8 could be the reaction products at the free carboxyl group at the D-Glu residue. It was reported that Bi_2WO_6 could generate positive holes and conduction band electrons under light irradiation (eq 1).[24] The photogenerated holes may attack the carboxyl group by the photo-Kolbe pathway to form a decarboxylation radical (eq 2).[35] The conduction band electron reacts with oxygen to form a superoxide radical (eq 3). In acidic solution, the $HO_2\bullet$ is formed (eq 4),[36] which could react with a decarboxylation radical quickly (eq 5) to form a hydroperoxide product m/z 513.8. However, this hydroperoxide product m/z 513.8 was not produced when P25 TiO_2 was used as catalyst. It was neither reported in other AOT processes, such as TiO_2 photocatalysis, BiOBr photocatalysis, sonolysis, or ozonation oxidizing.[14,21,22,37] This may be explained by the different active species responsible for the reactions. It was reported that the photocatalytic degradation by Bi_2WO_6 is mainly caused by photogenerated holes and superoxide radicals[24,26,28] while other AOT processes is dominated by •OH. The hydroperoxide product m/z 513.8 is further decomposed to a RO• radical and •OH under the irradiation (eq 6).[38] The RO• radicals undergo hydrogen atom abstraction to form the alcohol product m/z 505.8 (eq 7) and/or β-scission to yield a ketone product m/z 504.8 (eq 8).[38] These products could be further photodegraded to other small fragments. The proposed reaction pathway is shown in Figure 4.

$$Bi_2WO_6 \xrightarrow{\text{light}} h^+ + e_{CB}^- \quad (1)$$

$$R{-}COO^- + h^+ \rightarrow R\cdot + CO_2 \quad (2)$$

$$O_2 + e_{CB}^- \rightarrow O_2^{\cdot -} \quad (3)$$

$$O_2^{\cdot -} + H^+ \rightleftharpoons HO_2^{\cdot} \quad pKa = 4.8 \quad (4)$$

$$R^{\cdot} + HO_2^{\cdot} \rightarrow R{-}OOH \quad (5)$$

$$R{-}OOH \xrightarrow{h\nu} R{-}O\cdot + \cdot OH \quad (6)$$

$$R{-}O\cdot + \cdot H \rightarrow R{-}OH \quad (7)$$

$$R{-}O\cdot \xrightarrow{\beta\text{−scission}} R{=}O + \cdot H \quad (8)$$

The diene bond at the Adda chain is considered to be another active site for reaction. The intermediates at m/z 513.8, 505.8, and 504.8 could be further oxidized as diol products at the diene bonds, generating double charged species at m/z 530.8, 522.8, and 521.8, respectively (Supporting Information, Figure S11), which were observed in LC/MS as small peaks. The diol product m/z 522.8 could be further oxidized to produce a ketone at m/z 425.8. It is possible that the oxidation of the diene at Adda chain and the reaction at the Glu-carboxyl acid take place simultaneously.

There are two carboxyl groups in MC-RR: one is at the D-Glu residue and the other is at the MeAsp residue. The identified products suggest that the hydroperoxide reaction mainly happens at the D-Glu free carboxyl acid. When the concentration of MC-RR increased from 10 to 20 mg L^{-1}, an isomer of m/z 513.8 (isomer B) was detected with very low intensity. Isomer B eluted from the LC column earlier than the species at m/z 513.8 mentioned before, and they displayed different LC/MS/MS spectrum from isomer A (Supporting Information, Figure S5). The LC/MS/MS information indicates that isomer B of m/z 513.8 is the reaction product at the carboxyl group at MeAsp residue. This suggests that the D-Glu carboxyl acid is easier to be attacked than the MeAsp carboxyl acid. The results also support the assumption that MC-RR is adsorbed to the Bi_2WO_6 surface mainly at the side of the D-Glu residue.

Like other AOT processes, the conjugated carbon double bond and the aromatic ring of Adda in MCs are presumed to be active sites for reaction.[14,22,37,39] The intermediates at m/z 536.8 and 527.8 were identified as a diol and a phenol product, respectively, based on the results of LC/MS/MS, and they are considered to be the results of the reaction at the Adda chain. The detailed information about the identification of the species m/z 536.8 (Figures S12 and S13) and 527.8 (Figures S14 and S15) are

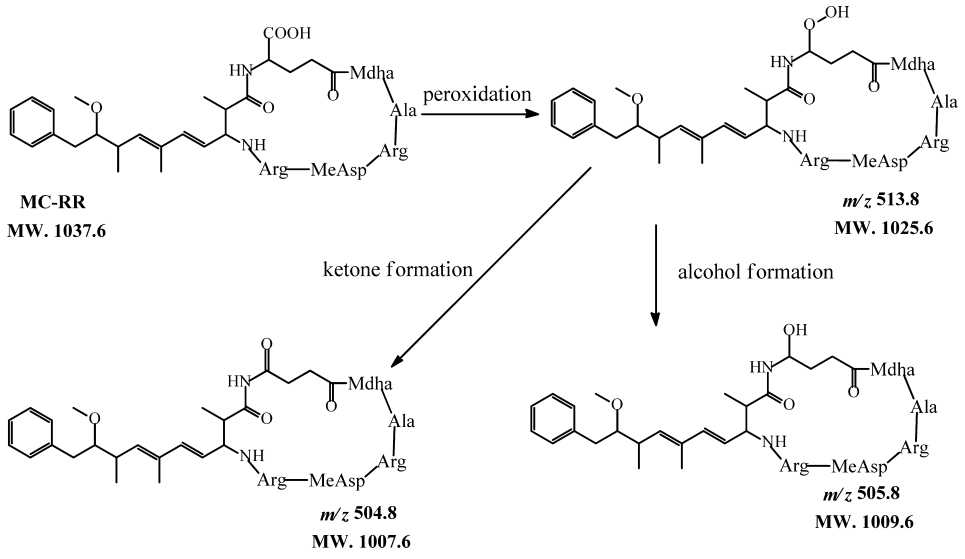

Figure 4. Possible photocatalytic degradation pathway of the free carboxyl group at the D-Glu site.

dx.doi.org/10.1021/es2036338 | Environ. Sci. Technol. 2012, 46, 2345−2351

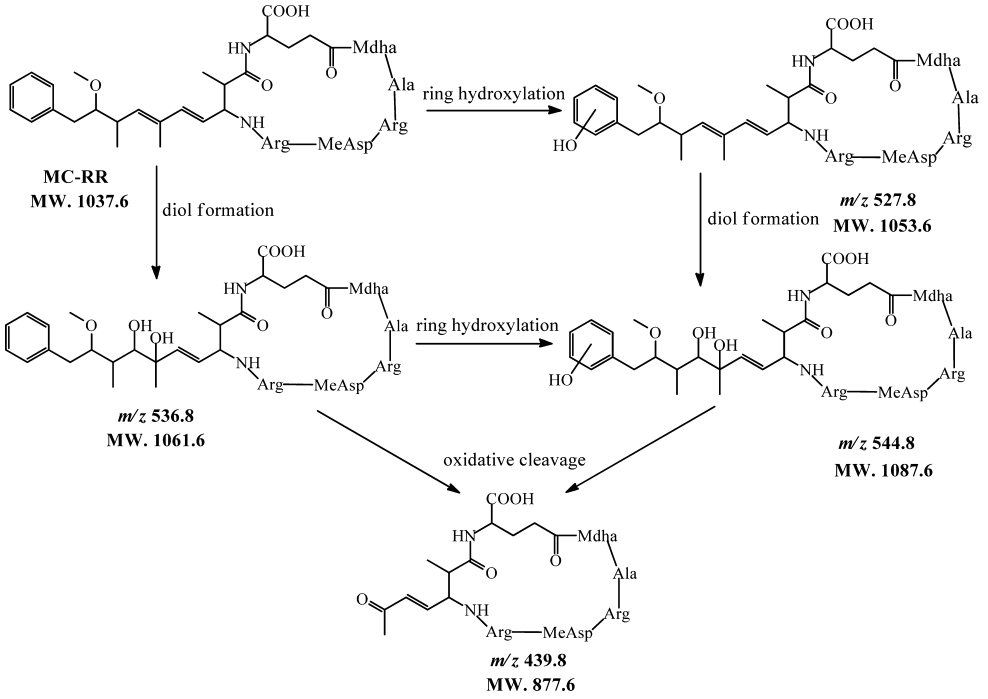

Figure 5. Possible photocatalytic degradation pathway of diene bond and aromatic ring of the Adda chain.

described in the Supporting Information. It is considered that the photogenerated holes could attack the diene bond or the aromatic ring, followed by the reactions with superoxide radicals. As a result, the diene bond is oxidized as a diol species with m/z 536.8, which could be further oxidized to ketone with m/z 439.8 (Supporting Information, Figures S16 and S17) by free radicals or photogenerated holes directly. The oxidation of the aromatic ring would result in the substitution of a hydrogen atom by a hydroxyl group, and a species at m/z 527.8 was formed. The proposed degradation pathway at the site of aromatic ring and diene bond is shown in Figure 5. These three intermediates (m/z 527.8, 536.8, and 544.8) were observed at the same time, suggesting that the reactions on the aromatic ring and the diene bond occur simultaneously.

■ ASSOCIATED CONTENT

Ⓢ Supporting Information

Detailed explanation of SEM images of Bi_2WO_6; peak areas, chromatographs by LC/MS, MS/MS spectrum, and structures of the main intermediates; and the possible pathway of degradation MC-RR. This material is available free of charge via the Internet at http://pubs.acs.org.

■ AUTHOR INFORMATION

Corresponding Author

*Phone: +86-22-23500791. Fax: +86-22-23503722. E-mail: zhuly@nankai.edu.cn.

■ ACKNOWLEDGMENTS

The authors gratefully acknowledge the financial support of Ministry of Education (Grant 708020); Tianjin Municipal Science and Technology Commission (10SYSYJC27200), Ministry of Science and Technology (2008ZX08526-003, 2009DFA91910, 2009BAC60B01), Ministry of Environmental Protection (201009026), and China−U.S. Center for Environmental Remediation and Sustainable Development.

■ REFERENCES

(1) Takenaka, S.; Watanabe, M. F. Microcystin LR degradation by *Pseudomonas aeruginosa* alkaline protease. *Chemosphere* **1997**, *34* (4), 749−757.

(2) Taylor, C.; Quinn, R. J.; Alewood, P. Synthesis of cyclic peptides modelled on the microcystin and nodularin rings. *Bioorg. Med. Chem. Lett.* **1996**, *6* (17), 2107−2112.

(3) Edwards, C.; Lawton, L. A.; Coyle, S. M.; Ross, P. Laboratory-scale purification of microcystins using flash chromatography and reversed-phase high-performance liquid chromatography. *J. Chromatogr., A* **1996**, *734* (1), 163−173.

(4) Imanishi, S.; Harada, K. Proteomics approach on microcystin binding proteins in mouse liver for investigation of microcystin toxicity. *Toxicon* **2004**, *43* (6), 651−659.

(5) Ziegmann, M.; Abert, M.; Müller, M.; Frimmel, F. H. Use of fluorescence fingerprints for the estimation of bloom formation and toxin production of *Microcystis aeruginosa*. *Water Res.* **2010**, *44* (1), 195−204.

(6) Cong, L.; Huang, B.; Chen, Q.; Lu, B.; Zhang, J.; Ren, Y. Determination of trace amount of microcystins in water samples using liquid chromatography coupled with triple quadrupole mass spectrometry. *Anal. Chim. Acta* **2006**, *569* (1−2), 157−168.

(7) Meriluoto, J.; Kurki-Helasmo, K. Microcystin uptake inhibits growth and protein phosphatase activity in mustard (*Sinapis alba* L.) seedlings. *Toxicon* **1998**, *36* (12), 1921−1926.

(8) Ito, E.; Takai, A.; Kondo, F.; Masui, H.; Imanishi, S.; Harada, K. Comparison of protein phosphatase inhibitory activity and apparent toxicity of microcystins and related compounds. *Toxicon* **2002**, *40* (7), 1017−1025.

(9) Lawton, L. A.; Robertson, P. K. J. Physico-chemical treatment methods for the removal of microcystins (cyanobacterial hepatotoxins) from potable waters. *Chem. Soc. Rev.* **1999**, *28* (4), 217−224.

(10) Harada, K.-i.; Tsuji, K.; Watanabe, M. F.; Kondo, F. Stability of microcystins from cyanobacteria—III.* Effect of pH and temperature. *Phycologia* **1996**, *35* (6S), 83−88.

(11) Gajdek, P.; Bober, B.; Mej, E.; Bialczyk, J. Sensitised decomposition of microcystin-LR using UV radiation. *J. Photochem. Photobiol., B* **2004**, *76* (1−3), 103−106.

(12) Feitz, A. J.; Waite, T. D. Kinetic modeling of TiO_2-catalyzed photodegradation of trace levels of microcystin-LR. *Environ. Sci. Technol.* **2003**, *37* (3), 561−568.
(13) Yuan, B. L.; Li, Y. B.; Huang, X. D.; Liu, H. J.; Qu, J. H. Fe(VI)-assisted photocatalytic degradating of microcystin-LR using titanium dioxide. *J. Photochem. Photobiol., A* **2006**, *178* (1), 106−111.
(14) Antoniou, M. G.; Shoemaker, J. A.; De La Cruz, A. A.; Dionysiou, D. D. Unveiling new degradation intermediates/pathways from the photocatalytic degradation of microcystin-LR. *Environ. Sci. Technol.* **2008**, *42* (23), 8877−8883.
(15) Lawton, L. A.; Robertson, P. K. J.; Cornish, B. J. P. A; Marr, I. L.; Jaspars, M. Processes influencing surface interaction and photocatalytic destruction of microcystins on titanium dioxide photocatalysts. *J. Catal.* **2003**, *213* (1), 109−113.
(16) Bandala, E. R.; Martínez, D.; Martínez, E.; Dionysiou, D. D. Degradation of microcystin-LR toxin by Fenton and photo-Fenton processes. *Toxicon* **2004**, *43* (7), 829−832.
(17) Song, W. H.; Teshiba, T.; Rein, K.; O'Shea, K. E. Ultrasonically induced degradation and detoxification of microcystin-LR (cyanobacterial toxin). *Environ. Sci. Technol.* **2005**, *39* (16), 6300−6305.
(18) Antoniou, M. G.; Nicolaou, P. A.; Shoemaker, J. A.; de la Cruz, A. A.; Dionysiou, D. D. Impact of the morphological properties of thin TiO_2 photocatalytic films on the detoxification of water contaminated with the cyanotoxin, microcystin-LR. *Appl. Catal., B* **2009**, *91* (1−2), 165−173.
(19) Graham, D.; Kisch, H.; Lawton, L. A.; Robertson, P. K. J. The degradation of microcystin-LR using doped visible light absorbing photocatalysts. *Chemosphere* **2010**, *78* (9), 1182−1185.
(20) Liu, I.; Lawton, L. A.; Cornish, B.; Robertson, P. K. J. Mechanistic and toxicity studies of the photocatalytic oxidation of microcystin-LR. *J. Photochem. Photobiol., A* **2002**, *148* (1−3), 349−354.
(21) Fang, Y. F.; Huang, Y. P.; Yang, J.; Wang, P.; Cheng, G. W. Unique ability of BiOBr to decarboxylate D-Glu and D-MeAsp in the photocatalytic degradation of microcystin-LR in water. *Environ. Sci. Technol.* **2011**, *45* (4), 1593−1600.
(22) Song, W.; De La Cruz, A. A.; Rein, K.; O'Shea, K. E. Ultrasonically induced degradation of microcystin-LR and -RR: Identification of products, effect of pH, formation and destruction of peroxides. *Environ. Sci. Technol.* **2006**, *40* (12), 3941−3946.
(23) Antoniou, M. G.; de la Cruz, A. A.; Dionysiou, D. D. Intermediates and reaction pathways from the degradation of microcystin-LR with sulfate radicals. *Environ. Sci. Technol.* **2010**, *44* (19), 7238−7244.
(24) Wang, C. Y.; Zhang, H.; Li, F.; Zhu, L. Y. Degradation and mineralization of bisphenol A by mesoporous Bi_2WO_6 under simulated solar light irradiation. *Environ. Sci. Technol.* **2010**, *44* (17), 6843−6848.
(25) Tang, J. W.; Zou, Z. G.; Ye, J. H. Photocatalytic decomposition of organic contaminants by Bi_2WO_6 under visible light irradiation. *Catal. Lett.* **2004**, *92* (1−2), 53−56.
(26) Fu, H. B.; Pan, C. S.; Yao, W. Q.; Zhu, Y. F. Visible-light-induced degradation of rhodamine B by nanosized Bi_2WO_6. *J. Phys. Chem. B* **2005**, *109* (47), 22432−22439.
(27) Zhu, S. B.; Xu, T. G.; Fu, H. B.; Zhao, J. C.; Zhu, Y. F. Synergetic effect of Bi_2WO_6 photocatalyst with C-60 and enhanced photoactivity under visible irradiation. *Environ. Sci. Technol.* **2007**, *41* (17), 6234−6239.
(28) Amano, F.; Nogami, K.; Ohtani, B. Visible light-responsive bismuth tungstate photocatalysts: effects of hierarchical architecture on photocatalytic activity. *J. Phys. Chem. C* **2009**, *113* (4), 1536−1542.
(29) Lopez-Ramon, M. V.; Stoeckli, F.; Moreno-Castilla, C.; Carrasco-Marin, F. On the characterization of acidic and basic surface sites on carbons by various techniques. *Carbon* **1999**, *37* (8), 1215−1221.
(30) Gao, C. M.; Wang, Z. Y.; Yu, Z. P.; Ye, B.; Liu, B.; Fan, X. P.; Qian, G. D. Effect of pH values on photocatalytic properties of Bi_2WO_6 synthesized by hydrothermal Method. *J. Wuhan Univ. Technol., Mater. Sci. Ed.* **2009**, *04*, 533−536.
(31) Fox, M. A.; Dulay, M. T. Heterogeneous photocatalysis. *Chem. Rev.* **1993**, *93* (1), 341−357.
(32) Hoffmann, M. R.; Martin, S. T.; Choi, W.; Bahnemann, D. W. Environmental applications of semiconductor photocatalysis. *Chem. Rev.* **1995**, *95* (1), 69−96.
(33) Huang, W. J.; Cheng, B. L.; Cheng, Y. L. Adsorption of microcystin-LR by three types of activated carbon. *J. Hazard. Mater.* **2007**, *141* (1), 115−122.
(34) Carraway, E. R.; Hoffman, A. J.; Hoffmann, M. R. Photocatalytic oxidation of organic acids on quantum-sized semiconductor colloids. *Environ. Sci. Technol.* **1994**, *28* (5), 786−793.
(35) Palominos, R.; Freer, J.; Mondaca, M. A.; Mansilla, H. D. Evidence for hole participation during the photocatalytic oxidation of the antibiotic flumequine. *J. Photochem. Photobiol., A* **2008**, *193* (2−3), 139−145.
(36) Bandara, J.; Kiwi, J. Fast kinetic spectroscopy, decoloration and production of H_2O_2 induced by visible light in oxygenated solutions of the azo dye Orange II. *New J. Chem.* **1999**, *23* (7), 717−724.
(37) Miao, H. F.; Qin, F.; Tao, G. J.; Tao, W. Y.; Ruan, W. Q. Detoxification and degradation of microcystin-LR and -RR by ozonation. *Chemosphere* **2010**, *79* (4), 355−361.
(38) Luengo, C.; Allen, N. S.; Edge, M.; Wilkinson, A.; Parellada, M. D.; Barrio, J. A.; Santa, V. R. Photo-oxidative degradation mechanisms in styrene-ethylene-butadiene-styrene (SEBS) triblock copolymer. *Polym. Degrad. Stab.* **2006**, *91* (4), 947−956.
(39) Liu, I.; Lawton, L. A.; Robertson, P. K. J. Mechanistic studies of the photocatalytic oxidation of microcystin-LR: An investigation of byproducts of the decomposition process. *Environ. Sci. Technol.* **2003**, *37* (14), 3214−3219.